Title page

Synergistic and independent roles for Nodal and FGF in zebrafish CPC migration and asymmetric heart morphogenesis

Vanessa Gonzalez[1†], Meagan G. Grant[1†], Makoto Suzuki[2], Briana Christophers[1], Jessica Rowland Williams[1#], Rebecca D. Burdine[1*]

[1] Department of Molecular Biology, Princeton University, Princeton, New Jersey, USA, 08544

[2] Amphibian Research Center, Graduate School of Integrated Sciences for Life, Hiroshima University, Higashihiroshima, Hiroshima, Japan, 739-8526.

[#] Current affiliation: National Institute for Student Success, Georgia State University, Atlanta, GA 30303

[†]These authors contributed equally to this work

***Correspondence should be addressed to this author at rburdine@princeton.edu**

Running Title: Nodal & FGF in Cardiac Morphogenesis

Key words: congenital heart defects, left-right asymmetry, cardiac looping, cardiac jogging, zebrafish

Summary statement

This study explores the synergistic and independent roles of Nodal and FGF signaling in generating heart asymmetry.

Abstract

Asymmetric development of the vertebrate heart is driven by a complex sequence of morphogenetic cell movements, coordinated through precise interpretation of signaling cues by the heart primordia. Here, we show that Nodal signaling functions synergistically with FGF to stimulate the migration of cardiac progenitor cells (CPCs) during cardiac jogging—the first morphological asymmetry observed in zebrafish heart development. While Nodal directs the asymmetric migration of CPCs, we find FGF signaling to be dispensable for this asymmetry, suggesting that FGF plays a permissive rather than instructive role. We further demonstrate that Nodal signaling induces asymmetries in actin cytoskeletal dynamics that correlate with the directional migration of CPCs, while FGF instead generally promotes the actin cytoskeleton of CPCs. In addition to influencing jogging, FGF and Nodal synergize to ensure proper heart looping. We also provide evidence that FGF contributes to heart looping by promoting the differentiation of the secondary heart field. Together, these findings offer insight into how the spatiotemporal dynamics of signaling pathways regulate the cellular behaviors driving organ morphogenesis.

Introduction

Vertebrate heart development requires the faithful execution of intricate and successive cell movements. The coupling of these movements to morphogenesis is mediated by the precise interpretation of signaling cues by heart primordia. Perturbations in these signaling pathways can underlie cellular processes that go awry in the roughly 40,000 infants born with a congenital heart defect (CHD) each year in the United States (Tsao et al., 2022). Therefore, a comprehensive analysis of signaling cues that direct cardiac cell behavior is critical for understanding the pathogenic mechanisms of CHDs.

The presence of conserved molecular mechanisms, the amenability to genetic manipulation and live imaging, and the ability for continued embryonic development in the presence of heart defects make zebrafish particularly advantageous for studying the cellular behaviors underlying cardiac morphogenesis (Bakkers, 2011; Genge et al., 2016; Grant et al., 2017; Nguyen et al., 2008; Smith and Uribe, 2021). During the initial stages of zebrafish heart development, CPCs are organized bilaterally within the anterior lateral plate mesoderm (LPM) as epithelial sheets, with ventricular progenitor positioned medial to atrial cells. These sheets converge on the embryonic midline, where they form the cardiac cone, a disc-shaped structure comprised of atrial cells at its base and ventricular cells at its apex (19 hours post fertilization, hpf; (Bakkers, 2011; Grant et al., 2017; Smith and Uribe, 2021).

During a process known as cardiac jogging, CPCs migrate in a leftward and anterior direction, with cells on the left half of the cardiac cone migrating more rapidly than the right-sided cells (20-24 hpf). This asymmetry in migration velocities results in clockwise rotation of the cardiac cone and displacement of atrial cells to the left and anterior of ventricular cells as the heart tube elongates. Cardiac jogging culminates in the asymmetric placement of the heart tube to the left of the embryonic midline, establishing the first asymmetry in the heart (Baker et al., 2008; de Campos-Baptista et al., 2008; Kidokoro et al., 2022; Lenhart et al., 2013; Rohr et al., 2008; Smith et al., 2008; Veerkamp et al., 2013). Post jogging, the second heart field is progressively added to the poles of the heart tube and contributes to heart tube elongation, eventually forming the outflow tract (24-48 hpf) (de Pater et al., 2009; Hami et al., 2011; Zhou et al., 2011). Between 30-48 hpf, the heart undergoes an evolutionarily conserved process known as cardiac looping. During this process, the heart tube bends rightward to begin defining and aligning the atrial and ventricular chambers of the heart, with actin polymerization being critical for dictating looping chirality (Desgrange et al., 2018; Noel et al., 2013; Smith and Uribe, 2021). Along with cardiac looping, the cardiac chambers undergo expansion and become morphologically discernible from one another via cardiac ballooning. Regionalized differences in cell morphology bring about chamber formation, and blood flow and contractility are critical for regulating these morphologies (Auman et al., 2007; Dietrich et al., 2014; Smith and Uribe, 2021).

Left-sided Nodal signaling in the LPM governs asymmetric behaviors during jogging and dextral looping of the heart. Nodal directs the asymmetric migration of CPCs during cardiac jogging by

68 increasing the velocities of left-sided cells in the cardiac cone and properly positioning the heart to the
69 left of the embryonic midline (Baker et al., 2008; de Campos-Baptista et al., 2008; Kidokoro et al., 2022;
70 Lenhart et al., 2013; Rohr et al., 2008; Veerkamp et al., 2013). While looping of the jogged heart tube
71 involves intrinsic mechanisms (Noel et al., 2013), this process is influenced by earlier Nodal signaling to
72 produce robustness in dextral looping morphogenesis (Grimes et al., 2020).
73 Although Nodal signaling is the dominant signal for sidedness, it is well-established that Nodal
74 signals integrate with other signaling pathways to orchestrate events controlling organogenesis (Hill,
75 2016; Massague, 2003). For example, during cardiac cone rotation and subsequent jogging, Nodal and
76 BMP signals act synergistically to influence cell migration (Lenhart et al., 2013; Veerkamp et al., 2013).
77 How other signaling pathways may integrate with Nodal signaling to orchestrate asymmetric heart
78 morphogenesis remains unknown.
79 Here, we characterize the synergistic and independent functions of Nodal and FGF signaling
80 during asymmetric morphogenesis of the zebrafish heart. We find FGF and Nodal both stimulate CPC
81 migration during cardiac jogging, but only Nodal is involved in directing asymmetric cell migration
82 suggesting that FGF plays a permissive role in this process. Consistent with these results, FGF
83 signaling promotes overall F-actin levels in CPCs while Nodal induces asymmetries in actin cytoskeletal
84 dynamics that correlate with directional migration of the CPCs. Later in development, FGF and Nodal
85 signals synergize to promote proper heart looping. We provide evidence that the role of FGF in cardiac
86 looping may be through promoting second heart field (SHF) addition to the ventricle, suggesting the
87 SHF promotes proper looping *in vivo*. Together, these findings shed insight into how Nodal and FGF
88 signals function to ensure proper migration and morphogenesis in the heart at multiple stages.
89
90 **Results**
91 **FGF and Nodal signals function synergistically during heart tube formation and jogging**
92 Previous studies have shown that the left-sided activation of Nodal in the anterior LPM drives
93 the directional migration of CPCs, determining the direction of heart tube displacement from the
94 embryonic midline during cardiac jogging (Baker et al., 2008; de Campos-Baptista et al., 2008;
95 Kidokoro et al., 2022; Lenhart et al., 2013; Rohr et al., 2008; Veerkamp et al., 2013). To understand
96 how Nodal influences left-right asymmetries in CPC migration, we analyzed our previous microarray
97 studies to identify cardiac-specific genes upregulated by Nodal signaling (Williams, 2015). Several
98 components of the FGF signaling pathway were upregulated in this analysis, including FGF receptors
99 *fgfr2*, *fgfr3*, and *fgfr4* and transcriptional targets of the pathway *erm*, *pea3*, and *spry4*. FGF signaling
100 components have been identified as Nodal targets during gastrulation in zebrafish, including *fgf17b*,
101 *fgf3*, and *fgf8* (Bennett et al., 2007). In zebrafish, *fgf8* is required for the development of cardiac
102 progenitor cells (CPCs) and is expressed in the cardiac cone prior to cardiac jogging (Fig. 1A; (Reifers
103 et al., 1998; Reifers et al., 2000). Given the recognized importance of FGF signaling in heart

development and the potential connection to Nodal, we tested whether FGF signaling contributed to heart jogging and looping, the two major left-right asymmetric events of the heart.

Since early inhibition of FGF signaling affects cardiac progenitor development (Felker et al., 2018; Marques et al., 2008; Reifers et al., 2000), we cannot make use of mutants such as *fgf8/ace* or global knockdown techniques to study later cardiac phenotypes. Thus, to inhibit FGF signaling with precise temporal control, we administered the pan-FGFR inhibitor SU5402 (Mohammadi et al., 1997). The addition of SU5402 at 24 hpf resulted in various cardiac defects, including severe pericardial edema and aberrant chamber placement, phenotypes associated with errors in the asymmetric development of the heart, suggesting FGF signaling could be involved in this process (Fig. 1B).

To confirm that inhibiting FGF signaling with SU5402 did not affect the establishment and expression of left-right patterning genes, we analyzed expression of the Nodal target gene *lefty2* in the cardiac cone. *lefty2* expression serves as both a readout of Nodal responsiveness and a direct readout of the sidedness of Nodal in the embryo (Fig. 1C). In WT embryos, *lefty2* expression is restricted to the left side of the cardiac cone (Fig. 1D). *southpaw* (*spaw*) mutants, which lack Nodal expression in the LPM, lack *lefty2* expression (Grimes et al., 2020; Noel et al., 2013), while the majority of *ntl* (*ntl/ntla/tbxta*) mutants, which have bilateral Nodal expression in the LPM, express *lefty2* bilaterally (Amack and Yost, 2004), as expected (Fig. 1D). Loss of FGF signaling in SU5402-treated WT embryos did not alter the left-sidedness of Nodal target *lefty2*, nor did loss of FGF change the expression profile of *lefty2* in *spaw* and *ntl* mutants (Fig. 1D). To corroborate our results with SU5402, we used the *Tg(hsp70l:dnfgfr1-EGFP)* heat shock inducible transgenic line to inhibit FGF signaling and found this similarly did not alter *lefty2* expression (Fig. 1D). These results suggest that any effect of FGF on asymmetric heart development is downstream of left-right axis establishment.

To investigate the role of FGF signaling during cardiac jogging—the first morphological sign of asymmetry in the embryo—we inhibited FGF using SU5402 or heat shock–induced dnFGFR1 from 19 hpf at cardiac cone formation, and continued treatment through jogging and heart tube formation (Fig. 2A). Embryos were fixed at 26.5 hpf and the laterality of heart jogging was analyzed (Fig. 2B). In WT embryos, heart tubes are displaced to the left of the embryonic midline, producing the expected “left jog” (Fig. 2C). Both *spaw* mutants and *ntl* mutants exhibit primarily “midline jog”, where the heart tube fails to be displaced to either side of the midline (Fig. 2C). Inhibiting FGF signaling in WT, *spaw* mutant, and *ntl* mutant embryos with either the pharmacological or heat shock approach did not affect laterality, as hearts jogged similarly to respective WT and mutant controls (Fig. 2C).

While the previous results suggest that FGF signaling does not influence jogging laterality, we observed that inhibition of FGF signaling led to fewer scorable hearts due to delayed tube formation, indicating a potential effect on CPC cell migration. To determine if FGF signaling affects cell migration during jogging, we inhibited FGF signaling at 18.5 hpf and assessed embryos at 24 hpf, a time when most wild-type (WT) embryos have completed jogging (Fig. 2D). *ntl* mutants exhibit only a slight delay

140 in cone-to-tube transition, compared to WT (Fig. 2E). By contrast, *spaw* mutants display a significant
141 delay in tube formation, with most hearts remaining at cone stage or starting to extend at 24 hpf (Fig.
142 2E). Both SU5402-treated and heat-shocked dnFGFR1 embryos display significant delays in tube
143 formation (Fig. 2E). Interestingly, treating *ntl* and *spaw* mutants with SU5402 further increased delays in
144 tube formation, with most hearts remaining in the cardiac cone stage (Fig. 2E). The strongest effect
145 was observed in *spaw* mutants treated with SU5402, in which all embryos analyzed remained at the
146 cardiac cone stage at 24 hpf (Fig. 2E). Taken together, these results suggest that both the Nodal and
147 FGF pathways promote CPC migration during jogging, leading to the formation of the heart tube at the
148 appropriate time.
149 To determine whether activating signaling downstream of FGF could restore CPC migration in
150 *spaw* mutants, we injected these mutants with photoswitchable MEK (psMEK). psMEK is active when
151 exposed to 500 nM light, activating the MAPK-ERK pathway which functions downstream of receptor
152 tyrosine kinases, including FGFR (Patel et al., 2019). When psMEK is activated during jogging, a
153 significantly higher number of embryos develop jogged and extended heart tubes compared to
154 untreated *spaw* mutants (Fig. 2E). However, jogging laterality was not rescued (Fig. 2C), suggesting
155 that while MAPK-ERK signaling enhances overall cell motility, it does not influence laterality.
156 While heart tube formation was delayed at 24 hpf in FGF-deficient and Nodal-deficient embryos,
157 heart tubes eventually formed in all groups after several additional hours but appeared shorter than
158 those in WT. To quantify this observation, we inhibited FGF during jogging and then measured heart
159 tube length at 26.5 hpf in embryos where the heart tube had completed jogging. Heart tubes were
160 significantly shorter in SU5402-treated embryos, possibly due to effects on the secondary heart field
161 (SHF) as reported previously (Fig. 2F; (de Pater et al., 2009; Felker et al., 2018; Lazic and Scott, 2011).
162 Heart tubes were also shorter in *spaw* mutants, suggesting that elongating in a midline position may be
163 inhibited by surrounding tissues (Fig. 2F). Combined loss of FGF and Nodal signaling (SU5402-treated
164 *spaw* mutants) was additive, producing significantly shorter heart tubes than *spaw* mutants or SU5402-
165 treated embryos (Fig. 2F). Overall, these data suggest that Nodal and FGF signaling synergize to
166 promote cell migration during heart tube formation and jogging, while only Nodal signaling is required to
167 induce lateralized migration during this process.
168
169 **Nodal and FGF signals regulate the velocity dynamics and directionality of CPCs during heart**
170 **tube formation**
171 Perturbation of the Nodal and FGF pathways results in defects in heart tube morphogenesis that
172 we hypothesize are due to defects in cell migration. To explore this possibility further, we conducted
173 confocal live imaging of embryos that express EGFP under the cardiac specific *myl7* promoter (Huang
174 et al., 2003) to quantify metrics of cell migration during jogging (Fig. 3A). Starting from the formation of
175 the cardiac cone, cell movements were analyzed for three hours in each condition. WT embryos

176 complete jogging within the three-hour time frame and formed a left-lateralized heart tube (Fig. 3B,
177 Movie 1). *ntl* mutants complete jogging in the same time frame but produce midline heart tubes due to
178 bilateral Nodal expression (Fig. 3B, Movie 2). *spaw* mutants also display midline heart tubes; however,
179 these CPCs migrated more slowly compared to WT or *ntl* mutants, often resulting in incomplete tube
180 extension during the three-hour time frame (Fig. 3B, Movie 3). Similarly, CPCs in SU5402-treated WT
181 embryos migrated more slowly compared to WT or *ntl* mutants, resulting in incomplete tube extension
182 during the imaging time frame (Fig. 3B, Movie 4). The effects of Nodal and FGF signaling on migration
183 are additive, as CPCs in SU5402-treated *spaw* mutants scarcely migrated during the same time (Fig.
184 3B, Movie 5).

185 To characterize asymmetric migration during jogging, we quantified the trajectories of the
186 outermost atrial CPCs, which display the largest disparity in left-right migration rates (Lenhart et al.,
187 2013) (Fig. 3C). Analysis of the direction and magnitude of CPC trajectories revealed that CPCs in WT
188 embryos exhibit a marked anterior and leftward displacement, while CPCs in *ntl* and *spaw* mutants fail
189 to undergo strong left or right displacement (Fig. 3D). Furthermore, in *ntl* and *spaw* mutants, overall
190 anterior displacement of CPCs was decreased (Fig. 3D). SU5402-treated embryos display a leftward
191 bias in CPC migration, though the overall displacement was not as marked as in WT embryos, and
192 anterior migration was reduced in these embryos (Fig. 3D). Both lateral and anterior migrations are
193 disrupted in SU5402-treated *spaw* mutants, further confirming that Nodal and FGF signals work
194 synergistically to promote CPC migration during jogging (Fig. 3D). The CPC trajectories further suggest
195 that Nodal and FGF signals contribute to the general anterior migration of the heart during jogging,
196 while asymmetric Nodal signals direct lateral migration.

197 To better understand the contributions of Nodal and FGF signals to cell migration, we analyzed
198 the migration velocities of CPCs. Cardiac laterality is known to be directed by left-right biases in cell
199 migration velocity driven by Nodal signaling, with left CPCs displaying a higher velocity than right CPCs
200 in WT embryos (de Campos-Baptista et al., 2008; Kidokoro et al., 2022; Lenhart et al., 2013; Veerkamp
201 et al., 2013). Given the bilateral exposure to Nodal of CPCs in *ntl* mutants, we expected migration to be
202 increased on both sides of the cardiac cone as we observed in *ntl* morphants (Lenhart K. F. et al.,
203 2013). However, we found that *ntl* mutants did not display increased migration velocities compared to
204 WT; nevertheless, the expected symmetry in migration velocities was observed (Fig. 3E). Consistent
205 with previous findings (de Campos-Baptista et al., 2008; Kidokoro et al., 2022; Lenhart et al., 2013;
206 Veerkamp et al., 2013), migration velocities of CPCs in *spaw* mutants are symmetric and reduced
207 compared to WT (Fig. 3E). Treatment with SU5402 in WT embryos produces a pronounced reduction
208 of migration velocity similar to that of *spaw* mutants (Fig. 3E). However, asymmetry in left versus right
209 migration velocities is still present, as expected given that heart tubes jog correctly to the left in these
210 embryos (Fig. 1D, 2C, 2F, 3E). Intriguingly, SU5402-treated *spaw* mutants display a more severe
211 reduction in migration velocity compared to *spaw* mutants or SU5402-treated embryos, further

212 suggesting synergy between Nodal and FGF signals in this process (Fig. 3E). Taken together, our
213 findings on CPC migration, velocity, and trajectories all support Nodal acting instructively to bias left
214 migration velocities, while FGF acts permissively and synergistically with Nodal to promote overall CPC
215 velocities during heart tube morphogenesis.
216
217 **Nodal induced asymmetries in actin polymerization correlate with left-right asymmetries in CPC**
218 **migration**
219 Cell migration is generally driven by dynamic assembly and disassembly of actin filaments
220 (Schaks et al., 2019). Since Nodal signaling can regulate actin during cardiac looping and other
221 developmental processes (Noel et al., 2013; Woo et al., 2012), we hypothesized that Nodal-driven
222 asymmetric migration of CPCs during jogging may also result in asymmetric actin dynamics. To assess
223 this possibility, we utilized the *Tg*(*myl7:Lifeact-EGFP*) transgenic, in which EGFP-labeled filamentous
224 actin (F-actin) is restricted to CPCs (Huang et al., 2003; Reischauer et al., 2014; Riedl et al., 2008),
225 permitting us to observe F-actin levels throughout jogging (Fig. 4A). Although CPCs migrate while
226 connected to their neighbors in an epithelial state (Trinh and Stainier, 2004), we observe dynamic
227 protrusions from individual cells during jogging (Fig. 4B, Movie 6). To our knowledge, this is the first
228 time the actin-rich protrusions of CPCs have been captured live during jogging, demonstrating the
229 strong migratory capacity of CPCs.
230 To determine how the actin dynamics in CPCs respond to Nodal signaling, we examined F-actin
231 dynamics in WT embryos and compared these dynamics to those of *ntl* morphants, *spaw* morphants,
232 and embryos treated with SB-505124, a pharmacological inhibitor of Nodal signaling (DaCosta Byfield
233 et al., 2004; Hagos and Dougan, 2007). In WT embryos, we find a stronger Lifeact/F-actin signal in left-
234 sided atrial cells of the cardiac cone compared to the corresponding right-sided cells, and this
235 asymmetry persists throughout jogging (Fig. 4C, Movie 7). Left-right asymmetry in F-actin is lost when
236 Nodal signaling is absent in *spaw* morphants or with administration of SB-505124. In fact, there was
237 minimal F-actin signal observed in the atrial cells of these embryos (Fig. 4D, Movies 8-9). Conversely,
238 we observe enrichment of F-actin in both left and right atrial cells in *ntl* morphants, in which Nodal is
239 expressed bilaterally in the LPM (Fig. 4D, Movie 10). To quantify these results, we measured the ratio
240 of fluorescence intensity values between left-sided and right-sided atrial cells (Fig. 4E). An intensity
241 ratio of left-to-right cells greater than 1 is indicative of left-biased levels, while an intensity ratio equal to
242 1 indicates symmetric levels. We found the fluorescence intensity ratio in WT embryos to be left-biased,
243 which is indicative of asymmetric F-actin levels (Fig. 4E; Table S1). However, *ntl* morphants, *spaw*
244 morphants, and SB505124-treated embryos had ratios indicative of symmetric F-actin levels (Fig. 4E).
245 Taken together, these findings suggest that asymmetries in Nodal correlate with asymmetries in F-actin
246 formation in migrating atrial CPCs, suggesting a possible mechanism by which Nodal could induce left-
247 right migration asymmetries in CPCs.

248 Given FGF inhibition reduces CPC migration velocity, we hypothesized this could also be due to
249 modulation of the actin cytoskeleton. We therefore treated *Tg(myl7:GFP-UtrCH)* embryos with SU5402
250 and imaged the resulting cardiac cone. GFP-UtrCH contains the utrophin calponin homology domain
251 fused to GFP to label F-actin. We find that CPCs in SU5402-treated embryos have reduced
252 fluorescence compared to WT embryos, suggesting that F-actin formation is reduced in FGF deficient
253 CPCs (Figure 4F-G, Table S2). This supports our previous data that FGF deficient CPCs migrate
254 slower and suggests a possible mechanism behind this observation.
255
256 **Proper cardiac looping requires FGF induction of the secondary heart field**
257 FGF signaling is known to influence various aspects of zebrafish heart morphogenesis, such as
258 CPC differentiation and proliferation, as well as chamber size and identity establishment (de Pater et
259 al., 2009; Felker et al., 2018; Lazic and Scott, 2011; Marques et al., 2008; Pradhan et al., 2017; Reifers
260 et al., 1998; Zeng and Yelon, 2014). In embryos treated with SU5402 from 24-48 hpf (continuous
261 treatment), differences in heart morphology between treated and WT embryos are apparent, particularly
262 defects in heart looping (Fig. 5A). Dextral heart looping is a highly conserved process in vertebrates
263 where the heart tube bends to place the chambers of the heart in their final, correct positions (Fig. 5B).
264 To determine if FGF signaling influences looping at a time point beyond jogging, we treated embryos
265 with SU5402 during specific developmental windows: during the heart tube elongation phase (24-30
266 hpf, prior to the onset of looping) and the heart tube bending phase (30-36 hpf, during looping) and
267 observed the resulting effects on hearts at 48 hpf (Fig. 5A). Given that FGF signaling did not influence
268 cardiac jogging laterality, we suspected that it would not influence looping laterality, as proper
269 lateralization of the heart during jogging promotes proper looping (Grimes et al., 2020). Accordingly,
270 embryos treated with SU5402 at either time point looped dextrally as expected (Fig. 5C).
271 Quantification of successful looping can be accomplished by measuring the looping angle: the
272 angle formed by the intersection of a line along the anterior-posterior axis and a line through the
273 atrioventricular canal (AVC) at 48 hpf (Fig. 5B), with a properly developed heart having a looping angle
274 of ~25.0° (Chernyavskaya et al., 2012). In WT embryos, the heart completes looping and the atrium
275 and ventricle are correctly positioned side-by-side at 48 hpf (Fig. 5B). Quantification of looping angle in
276 WT *Tg(myl7:EGFP)* embryos yields a mean looping angle of 25.0° (Fig. 5D). Despite not altering
277 looping laterality, SU5402 treatment did result in errors in looping angle. Treatment with SU5402 during
278 the elongation phase results in significantly larger looping angles, suggesting looping is impaired when
279 FGF signaling is inhibited prior to the start of looping (Fig. 5B, 5D). Treatment during the bending phase
280 does not affect looping angles, indicating that inhibition of FGF signaling during the start of looping
281 does not impair the process (Fig. 5B, 5D). Heart looping is compromised in *spaw* mutants, as expected
282 given Nodal is known to be necessary for robust looping (Grimes et al., 2020; Noel et al., 2013) (Fig.
283 5B, 5D). We found that loss of FGF signaling during the elongation phase in *spaw* mutants exacerbated

284 heart looping defects as quantified by looping angle (Fig. 5B, 5D). Our results suggest that Nodal and
285 FGF synergize to promote heart looping.
286 It is known that FGF signaling is necessary for the differentiation and addition of the SHF to the
287 arterial pole of the heart tube in zebrafish post 24 hpf (de Pater et al., 2009; Felker et al., 2018; Lazic
288 and Scott, 2011). We hypothesized that inhibition of FGF from 24 to 30 hpf in our study may prevent
289 development of the SHF, which may in turn influence heart looping. To test our hypothesis, we treated
290 *Tg(nkx2.5:ZsYellow)* embryos with SU5402 during the elongation phase and measured the elongating
291 heart tube at both 26.5 and 28 hpf. *Tg(nkx2.5:ZsYellow)* marks both the first and second heart fields,
292 and absence of the SHF can be visualized as a shorter heart tube (Nevis et al., 2013). Measuring heart
293 tube length revealed significantly shorter heart tubes in SU5402-treated embryos at both time points,
294 likely due to the loss of the SHF (Fig. 5E).
295 To further test whether the effect on heart looping we observe is due to loss of the SHF, we
296 inhibited SHF development by injecting embryos with a morpholino against *ltbp3* as described (Zhou et
297 al., 2011). Similar to embryos treated with SU5402 from 24-30 hpf, *ltbp3* morphants exhibit comparable
298 defects in looping angle (Fig. 5B, 5D). Taken together, these data suggest that inhibiting FGF signaling
299 from 24-30 hpf affects proper cardiac looping through loss of the SHF.
300
301 **Discussion**
302 **Nodal and FGF signals function synergistically to promote migration underlying cardiac jogging**
303 **and tube extension**
304 Our results show that both Nodal and FGF signals promote overall cell migration during heart
305 tube formation and asymmetric placement. Losing either signal reduces cell velocities in the cone and
306 delays the cone-to-tube transition compared to WT, while losing both signals more severely perturbs
307 CPC migration and tube formation. During jogging, our data suggests that FGF signals act permissively
308 to promote motility, while Nodal signals act instructively to direct CPC laterality (Fig. 6). FGF signaling
309 is known to cooperate with Nodal signaling in coupling cell migration in various morphogenetic events,
310 including in the *Ciona* neural tube and the zebrafish brain (Navarrete and Levine, 2016; Regan et al.,
311 2009; Roussigne et al., 2018). Intriguingly, in the zebrafish brain, FGF and Nodal signaling function
312 together to control left-right asymmetry by mediating collective cell migration; Nodal restricts and biases
313 the activation of FGF to leading parapineal cells, resulting in a leftward, asymmetric migration (Regan
314 et al., 2009; Roussigne et al., 2018). FGF is critical for parapineal cell migration, but Nodal signaling
315 directs the laterality of this movement. This is in line with our findings that FGF is critical for overall CPC
316 migration while Nodal directs the laterality of CPC movements.
317 We also find that Nodal and FGF synergize to affect the length of the heart tube at 24 hpf
318 following jogging. Whether this defect is only the consequence of compromised motility, or whether
319 there are other forces that restrict elongation, remains to be determined. For example, the defects we

320 observe are highly reminiscent of *heart and mind* (*had*) and *heart and soul* (*has*) mutants, which have
321 reduced heart tube extension (Rohr et al., 2006; Shu et al., 2003). Interestingly, *had* and *has* encode
322 regulators of epithelial polarity, the establishment and maintenance of which is crucial for proper
323 cardiac morphogenesis. Interrogating epithelial polarity and cell shape changes under the conditions in
324 our study may prove informative in understanding heart tube extension. Alternatively, the decrease in
325 heart tube length we observe in our study conditions could be due to tissue constraints on the tube as it
326 attempts to elongate closer to the midline. Future studies are needed to determine what drives the
327 overall anterior displacement of the heart cone/tube and the forces that drive tube extension during
328 development.
329
330 **Nodal signals induce left-right asymmetries in F-actin that correlate with asymmetric migration**
331 We demonstrate that Nodal signaling induces an increase in F-actin levels in migrating left atrial
332 cells that is not observed in right atrial cells. This increase in F-actin is Nodal dependent, as it is lost in
333 embryos injected with *spaw* morpholino or treated with Nodal inhibitor. In agreement, in embryos
334 injected with *ntl* morpholino, where Nodal signals to both sides of the cardiac cone, both left and right
335 atrial cells show increases in F-actin. This suggests that Nodal induces asymmetric migration by
336 increasing actin dynamics within left atrial cells, which migrate faster than their counterparts on the
337 right, driving clockwise rotation of the cone. Previous studies have suggested roles for Nodal in
338 inducing cytoskeletal rearrangements in migrating cells (Noel et al., 2013; Schier, 2009; Woo et al.,
339 2012) lending support to our hypothesis.
340 The cells in the cone are epithelial and migrate collectively during jogging. Intriguingly, using
341 mosaic labeling with our Lifeact reporter, we observed highly dynamic, protrusive F-actin activity in
342 these left-sided migrating cells. It is intriguing to speculate that these are “cryptic” basal extensions that
343 are driving migration similar to what has been observed in cultured MDCK kidney cells during wound
344 healing (Farooqui and Fenteany, 2005). Future studies can determine if these protrusions are basal-to-
345 junctional complexes coming only from edge cells or if additional cells deeper in this epithelium are
346 helping drive migration.
347 We also demonstrate that the reduced migration rates seen in SU5402-treated embryos could
348 be due to a reduction of F-actin throughout the cardiac cone. Given Nodal expression is unaltered in
349 this condition, and the heart migrates towards the left, we hypothesize that F-actin asymmetry would
350 not be lost in FGF deficient embryos. This could be assessed in the future with appropriate transgenic
351 lines. Future studies can further delve into how loss of FGF affects CPC migration at the cellular level.
352
353 **FGF signaling is necessary for proper cardiac looping**
354 Extending our studies with the FGF inhibitor SU5402, we find that treatment with SU5402 from
355 24 to 30 hpf (during heart tube elongation) affected cardiac looping and final chamber placement, while

356 treatment from 30 to 36 hpf (during heart tube looping) did not affect looping (Fig. 6). This suggests that
357 FGF continues to play important roles in asymmetric heart morphogenesis after jogging is complete.
358 Cardiac looping is a highly conserved event in vertebrate heart development, but much remains to be
359 discovered regarding its underlying mechanisms. We previously reported that jogging correctly
360 increases the correct dextral loop in the heart, suggesting that the first asymmetric migration at 20 hpf
361 still provides input to heart-intrinsic chirality mechanisms at later stages (Grimes et al., 2020). Our work
362 here suggests that at least one additional input into looping *in vivo* involves FGF. We provide evidence
363 that this input may be through SHF addition given the similarity in phenotypes between *ltbp3* morphants
364 and SU5402-treated embryos, both of which lack SHF structures. This is further supported by work
365 showing heart looping defects in *isl2a* and *isl2b* mutant embryos, which produce defects in the SHF
366 (Witzel et al., 2017). Biomechanical modeling also suggests that it is the rotation of the poles of the
367 heart tube that drives looping, and a lack of SHF would prevent this rotation from occurring properly
368 (Manner, 2004). Determining how the SHF contributes to proper heart looping in zebrafish will be an
369 important area for future studies. Intriguingly, we show that Nodal and FGF both promote heart looping,
370 as losing both pathways produces more severe defects in this process than losing either alone.
371
372 **Concluding remarks and future directions**
373 Here, we highlight molecular mechanisms through which the spatiotemporal dynamics of
374 signaling cues influence cardiac progenitor cell behaviors and heart morphogenesis. We further show
375 that the differential effects exerted by interacting signals on CPCs manifest as dramatic asymmetries in
376 heart tube morphogenesis, highlighting the fact that earlier patterning events regulate morphogenetic
377 processes occurring later in development.
378 Our study suggests areas of future research on how signaling pathways synergize to promote
379 morphogenesis. In addition to the ideas already discussed, we note that while jogging was most
380 significantly delayed in embryos lacking both Nodal and FGF, heart tubes nevertheless ultimately
381 formed, raising the question of what additional signals govern tube formation under these conditions.
382 We also don't have evidence as to whether the effect of FGF signaling on CPC migration is direct or
383 indirect. We hypothesize it will be direct given we and others have shown that FGF components, like
384 *fgf8*, are expressed in the early heart. Transgenic lines that modulate FGF signaling specifically in the
385 myocardium could provide clues as to how FGF influences the CPCs during jogging and looping.
386 We note that the decreased velocity we observe here in *ntl* mutants conflicts with our previously
387 published data using *ntl* morphants, in which we observed higher velocities in CPCs compared to WT
388 (Lenhart et al., 2013). It is possible that there may be an unexpected difference in *ntl* mutants versus
389 morphants that produces this discrepancy (Stainier et al., 2017). However, distinct microscopes,
390 acquisition parameters, and analysis software were utilized in this study could also account for
391 differences in velocity values, compared to our previous publication.

392 Ultimately, further interrogation of the roles of Nodal and FGF signaling throughout heart
393 morphogenesis will prove informative in understanding how signaling and cellular aberrancies manifest
394 as morphological defects. Given heart tube malformations are among the most commonly diagnosed
395 congenital heart defects, knowing how they arise is crucial for reducing the mortality and morbidity
396 associated with CHDs.
397
398
399 **Materials and methods**
400 **Zebrafish strains**
401 All experimental procedures in this study were conducted in accordance with the Princeton University
402 Institutional Animal Care and Use Committee. Zebrafish (*Danio rerio*) embryos were maintained at
403 28°C and grown in E3 embryo medium (5 mM NaCl, 0.17 mM KCl, 0.33 mM $CaCl_2$, 0.33 mM $MgSO_4$).
404 We used wild-type strains WIK and PWT. We used the zebrafish mutants *ntl*^{b160} and *spaw*^{sa177} (Grimes
405 et al., 2020; Halpern et al., 1993). We used the transgenic strains *Tg(myl7:EGFP)twu34* (Huang et al.,
406 2003)*, TgBAC(-36nkx2.5:ZsYellow)fb7* (Zhou et al., 2011)*,* and *Tg(hsp70l:dnfgfr1a-EGFP)pd1;* (Lee et
407 al., 2005).
408
409 **Generation of transgenic line**
410 We generated the *Tg(myl7:Lifeact-EGFP)pr26* and *Tg(myl7:GFP-UtrCH)pr27* transgenic strains using
411 the Tol2 transposase system (Kawakami, 2007). Briefly, 1-cell stage embryos were injected with Tol2
412 mRNA and *pTol2005b-myl7:Lifeact-EGFP* or *pTol2005b-myl7:GFP-UtrCH* plasmid. Only correctly
413 developing embryos with EGFP-positive hearts were raised. Injected F_0 fish were outcrossed to
414 generate stable transgenic lines.
415
416 **Drug treatments**
417 A 10 mM stock of the FGFR inhibitor SU5402 (Sigma-Aldrich) in DMSO was diluted to a working
418 concentration of 6 μM or 10 μM in a 1% DMSO/1X E3 solution. 6 μM was used for inhibition during
419 bending and elongation phases and 10 μM was used for inhibition during jogging phase. Embryos were
420 incubated at 28°C in the dark for varying durations of time: 18.5-24 hpf, 24-30 hpf, and 30-36 hpf. In our
421 experiments, expression of the FGF signaling targets *pea3* and *erm* is lost within 30 minutes of
422 treatment initiation. Upon completion of SU5402 incubation, embryos underwent live imaging or were
423 fixed in 4% paraformaldehyde (PFA; Electron Microscopy Sciences) for RNA *in situ* analysis. Due to the
424 light-sensitivity of SU5402, treated embryos were incubated in the dark. For SB-505124 (Sigma-Aldrich)
425 treatments, a 10 mM stock in DMSO was diluted to a working concentration of 40 μM and administered
426 to embryos at the tailbud stage; embryos then underwent live imaging during jogging as described

427 (Lenhart et al., 2013). Note that DMSO-treated vehicles did not differ from WT embryos in the
428 processes studied.
429
430 **Heat shock treatment**
431 *Tg(hsp70l:dnfgfr1-EGFP)pd1* embryos underwent heat shock at 38°C for 30 minutes every 2 hours
432 from 17 hpf until fixation to ensure FGF inhibition during jogging phase. The dominant negative FGF
433 construct has been found to activate approximately 2 hours post initial heat shock (Lee et al., 2014;
434 Pouget et al., 2014; Vemaraju et al., 2012). Thus starting heat shock at 17 hpf allowed for FGF
435 inhibition in the same time window as in our experiments with SU5402. EGFP expression served as
436 confirmation of successful heat shock. Hearts at 26.5 hpf appeared comparable to WT in shape and
437 size, indicating CPC differentiation was not affected by treatment during this timeframe.
438
439 **RNA and morpholino injections**
440 psMEK mRNA injections were performed as previously described (Patel et al., 2019). Briefly, 50 pg of
441 psMEK^{E203K} mRNA was injected into the yolk at the 1-cell stage. Injected embryos were immediately
442 placed in a dark box until 18.5 hpf. The lid of the box was then removed and replaced with a LED board
443 emitting 505 nm light from 18.5 to 24 hpf to activate MEK signaling during jogging phase. Morpholino
444 injections were performed as previously described using established morpholinos for *spaw*, *ntl*, and
445 *ltbp3* (Lenhart et al., 2013; Long et al., 2003; Nasevicius and Ekker, 2000; Zhou et al., 2011). Note that
446 control embryos injected with phenol red and nuclease-free water for both psMEK and morpholino
447 injections did not differ from WT embryos in the processes studied.
448
449 **RNA *in situ* hybridization**
450 Chromogenic whole-mount RNA *in situ* hybridization was performed using digoxygenin-labeled RNA
451 probes for *myl7* and *lefty2* (Berdougo et al., 2003; Bisgrove et al., 1999; Thisse and Thisse, 2014;
452 Yelon et al., 1999). Images were acquired using the Leica DMRA microscope. Fluorescent whole-
453 mount *in situ* hybridization was performed using the Molecular Instruments HCR kit as described (Choi
454 et al., 2018) for probes against *myl7* and *fgf8*. Images were acquired using the Nikon A1 confocal
455 microscope.
456
457 **Confocal imaging and analysis**
458 To analyze cell migration during cardiac jogging, dechorionated embryos were mounted in 0.8%
459 low-melt agarose as previously described (Lenhart et al., 2013). The dish was covered with a 0.5%
460 DMSO/1X E3 solution containing 0.13 mM tricaine (MS-222; Sigma-Aldrich). For SU5402 treatments, a
461 5 μM dilution in 0.8% agarose was used for mounting embryos, which were incubated in inhibitor at

462 least 30 minutes before mounting and covered with 10 μM inhibitor in 0.5% DMSO/1X E3 containing
463 0.13 mM tricaine.
464 For analysis of cardiac cell movements, embryos were imaged from 18-24 hpf using a Leica
465 SP5 confocal microscope. The Leica Mark & Find feature was used to image up to 4 embryos per
466 imaging session for higher throughput. A heated stage set to 28.5°C was used, which permitted
467 imaging for several hours without perturbing development.
468 We acquired confocal z-stacks at 4- or 5-minute intervals with a spacing of 2 μm. To track
469 individual cells during jogging, we compressed the z-stacks into a single dimension and then utilized
470 the ImageJ program TrackMate to track and quantify metrics of each cell during its migration. To
471 ensure consistent quantification of velocity over time between different genotypes, we tracked CPCs
472 over the same developmental window: we began tracking cells upon anterior fusion of CPCs at the
473 midline and ended tracking 3 hours thereafter. Note that only outer, atrial cells were chosen for tracking
474 as they undergo the most migration during jogging; the bright ventricular cells around the lumen are
475 excluded from analysis (Lenhart et al., 2013). Average velocity and angle of displacement for each cell
476 were calculated using raw position, displacement, and time measurements generated by TrackMate.
477 Resulting cell velocities, angles, and displacements were input into Prism or RStudio for analysis. Note
478 that distinct microscopes, acquisition parameters, and analysis software were utilized and may account
479 for differences in velocity values, compared to our previous publications.
480 For analysis of F-actin in *Tg(myl7:Lifeact-EGFP)pr26* embryos, embryos were mounted and
481 handled as described above. Embryos were imaged from 19-23 hpf using a Prairie Ultima two-photon
482 microscope. Z-stacks were acquired at 15-minute intervals with a spacing of 4 μm. Fluorescence
483 intensity analysis was performed using ImageJ.
484 For analysis of F-actin in *Tg(myl7:GFP-UtrCH)pr27* embryos, embryos were dechorionated and
485 fixed in 4% PFA with 4% sucrose and fixed overnight at 4°C. Embryos were then washed four times
486 with PBS-Tween and then transferred to 30% glycerol and then 50% glycerol in PBS-Tween. Embryos
487 were then deyolked, mounted, and imaged using a Nikon A1R-Si confocal microscope. The 40X
488 objective was used and Z-stacks had a spacing of 1 μm. Fluorescence intensity analysis was
489 performed using ImageJ.
490 For observing cardiac looping, embryos were mounted and handled as described above.
491 Images were acquired using the Leica M205 FA fluorescent stereoscope.
492
493 **Heart measurements and scoring**
494 For observing heart tube length in fixed embryos processed via RNA *in situ* hybridization,
495 embryos were observed using the Leica S6E dissecting microscope and heart tube length was
496 measured through the eyepiece using an ocular micrometer and a stage micrometer. For observing
497 heart tube length and cardiac looping in live embryos, embryos were mounted and handled as

498 described above. Images were acquired using the Leica M205 FA fluorescent stereoscope. Analysis
499 was performed using ImageJ ruler and angle tools. The looping angle is defined as the angle between
500 the plane of the anterior-posterior axis and the AVC (Chernyavskaya et al., 2012).
501 For scoring of heart laterality, embryos were staged at 26.5 hpf and scored as previously
502 described (Grimes et al., 2020; Lenhart et al., 2013). Briefly, the heart tubes of embryos were
503 viewed dorsally using a stereomicroscope. A heart tube that remained along the midline was scored
504 as midline; a tube that deviated from the midline was scored as having jogged left or right.
505
506 **Statistical analysis**
507 All bar graphs were generated using GraphPad Prism 9.4.0. Statistical tests of significance (Student's t-
508 test, Chi-square analysis) were calculated using GraphPad Prism analysis software. Note at least N = 2
509 biological and technical replicates were performed for each experiment.
510
511 **Acknowledgments**
512 We would like to thank Dr. Kenneth Poss, Dr. Stefano Di Talia, Dr. Tatjana Piotrowski, and Dr. C. Ben
513 Lovely for providing us with zebrafish transgenic strains to conduct this work. We thank Dr. Gary
514 Laevsky and the Confocal Imaging Facility, a Nikon Center of Excellence, in the Department of
515 Molecular Biology for their assistance with imaging. We also thank Phillip Johnson and his team for
516 their assistance with fish husbandry.
517
518 **Competing Interests**
519 The authors declare that they have no competing interests.
520
521 **Funding**
522 M.S. was a visiting scientist supported by the Strategic International Research Exchange Program
523 between Princeton University and National Institutes of Natural Sciences, Japan. Research reported in
524 this manuscript was supported by a National Science Foundation under grant IOS-1147123 to RDB and
525 a predoctoral fellowship to JRW; a Janssen Scholars of Oncology Diversity Engagement Fellowship to
526 and an American Heart Association Predoctoral Fellowship 24PRE1198653 to VG; grant
527 R01HD048584 from the National Institutes of Child Health and Human Development and
528 COCR24PRG007 from the New Jersey Commission on Cancer Research to RDB, and grant
529 T32GM007388 from the National Institute of General Medical Sciences to JRW. The content is solely
530 the responsibility of the authors and does not necessarily represent the official views of the National
531 Institutes of Health.
532
533 **Data and resource availability**

All relevant data and resources can be found within the article and its supplementary information. The data that support the findings of this study are available from the corresponding author RDB, upon reasonable request.

Diversity and inclusion statement

One or more of the authors of this paper self-identifies as an underrepresented ethnic minority in science. One or more of the authors of this paper self-identifies as living with a disability. One or more authors of this paper received support from a program designed to increase minority representation in science. Five of the six authors on this paper are women, who are often underrepresented in science.

References

Amack, J. D. and Yost, H. J. (2004). The T box transcription factor no tail in ciliated cells controls zebrafish left-right asymmetry. *Curr Biol* **14**, 685-690.

Auman, H. J., Coleman, H., Riley, H. E., Olale, F., Tsai, H. J. and Yelon, D. (2007). Functional modulation of cardiac form through regionally confined cell shape changes. *PLoS Biol* **5**, e53.

Baker, K., Holtzman, N. G. and Burdine, R. D. (2008). Direct and indirect roles for Nodal signaling in two axis conversions during asymmetric morphogenesis of the zebrafish heart. *Proc Natl Acad Sci U S A* **105**, 13924-13929.

Bakkers, J. (2011). Zebrafish as a model to study cardiac development and human cardiac disease. *Cardiovasc Res* **91**, 279-288.

Bennett, J. T., Joubin, K., Cheng, S., Aanstad, P., Herwig, R., Clark, M., Lehrach, H. and Schier, A. F. (2007). Nodal signaling activates differentiation genes during zebrafish gastrulation. *Dev Biol* **304**, 525-540.

Berdougo, E., Coleman, H., Lee, D. H., Stainier, D. Y. and Yelon, D. (2003). Mutation of weak atrium/atrial myosin heavy chain disrupts atrial function and influences ventricular morphogenesis in zebrafish. *Development* **130**, 6121-6129.

Bisgrove, B. W., Essner, J. J. and Yost, H. J. (1999). Regulation of midline development by antagonism of lefty and nodal signaling. *Development* **126**, 3253-3262.

Chernyavskaya, Y., Ebert, A. M., Milligan, E. and Garrity, D. M. (2012). Voltage-gated calcium channel CACNB2 (beta2.1) protein is required in the heart for control of cell proliferation and heart tube integrity. *Dev Dyn* **241**, 648-662.

Choi, H. M. T., Schwarzkopf, M., Fornace, M. E., Acharya, A., Artavanis, G., Stegmaier, J., Cunha, A. and Pierce, N. A. (2018). Third-generation in situ hybridization chain reaction: multiplexed, quantitative, sensitive, versatile, robust. *Development* **145**.

DaCosta Byfield, S., Major, C., Laping, N. J. and Roberts, A. B. (2004). SB-505124 is a selective inhibitor of transforming growth factor-beta type I receptors ALK4, ALK5, and ALK7. *Mol Pharmacol* **65**, 744-752.

de Campos-Baptista, M. I., Holtzman, N. G., Yelon, D. and Schier, A. F. (2008). Nodal signaling promotes the speed and directional movement of cardiomyocytes in zebrafish. *Dev Dyn* **237**, 3624-3633.

de Pater, E., Clijsters, L., Marques, S. R., Lin, Y. F., Garavito-Aguilar, Z. V., Yelon, D. and Bakkers, J. (2009). Distinct phases of cardiomyocyte differentiation regulate growth of the zebrafish heart. *Development* **136**, 1633-1641.

Desgrange, A., Le Garrec, J. F. and Meilhac, S. M. (2018). Left-right asymmetry in heart development and disease: forming the right loop. *Development* **145**.

Dietrich, A. C., Lombardo, V. A., Veerkamp, J., Priller, F. and Abdelilah-Seyfried, S. (2014). Blood flow and Bmp signaling control endocardial chamber morphogenesis. *Dev Cell* **30**, 367-377.

Farooqui, R. and Fenteany, G. (2005). Multiple rows of cells behind an epithelial wound edge extend cryptic lamellipodia to collectively drive cell-sheet movement. *J Cell Sci* **118**, 51-63.

Felker, A., Prummel, K. D., Merks, A. M., Mickoleit, M., Brombacher, E. C., Huisken, J., Panakova, D. and Mosimann, C. (2018). Continuous addition of progenitors forms the cardiac ventricle in zebrafish. *Nat Commun* **9**, 2001.

Genge, C. E., Lin, E., Lee, L., Sheng, X., Rayani, K., Gunawan, M., Stevens, C. M., Li, A. Y., Talab, S. S., Claydon, T. W., et al. (2016). The Zebrafish Heart as a Model of Mammalian Cardiac Function. *Rev Physiol Biochem Pharmacol* **171**, 99-136.

Grant, M. G., Patterson, V. L., Grimes, D. T. and Burdine, R. D. (2017). Modeling Syndromic Congenital Heart Defects in Zebrafish. *Curr Top Dev Biol* **124**, 1-40.

Grimes, D. T., Patterson, V. L., Luna-Arvizu, G., Schottenfeld-Roames, J., Irons, Z. H. and Burdine, R. D. (2020). Left-right asymmetric heart jogging increases the robustness of dextral heart looping in zebrafish. *Dev Biol* **459**, 79-86.

Hagos, E. G. and Dougan, S. T. (2007). Time-dependent patterning of the mesoderm and endoderm by Nodal signals in zebrafish. *BMC Dev Biol* **7**, 22.

Halpern, M. E., Ho, R. K., Walker, C. and Kimmel, C. B. (1993). Induction of muscle pioneers and floor plate is distinguished by the zebrafish no tail mutation. *Cell* **75**, 99-111.

Hami, D., Grimes, A. C., Tsai, H. J. and Kirby, M. L. (2011). Zebrafish cardiac development requires a conserved secondary heart field. *Development* **138**, 2389-2398.

Hill, C. S. (2016). Transcriptional Control by the SMADs. *Cold Spring Harb Perspect Biol* **8**.

Huang, C. J., Tu, C. T., Hsiao, C. D., Hsieh, F. J. and Tsai, H. J. (2003). Germ-line transmission of a myocardium-specific GFP transgene reveals critical regulatory elements in the cardiac myosin light chain 2 promoter of zebrafish. *Dev Dyn* **228**, 30-40.

Kawakami, K. (2007). Tol2: a versatile gene transfer vector in vertebrates. *Genome Biol* **8 Suppl 1**, S7.

Kidokoro, H., Saijoh, Y. and Schoenwolf, G. C. (2022). Nodal signaling regulates asymmetric cellular behaviors, driving clockwise rotation of the heart tube in zebrafish. *Commun Biol* **5**, 996.

Lazic, S. and Scott, I. C. (2011). Mef2cb regulates late myocardial cell addition from a second heart field-like population of progenitors in zebrafish. *Dev Biol* **354**, 123-133.

Lee, Y., Grill, S., Sanchez, A., Murphy-Ryan, M. and Poss, K. D. (2005). Fgf signaling instructs position-dependent growth rate during zebrafish fin regeneration. *Development* **132**, 5173-5183.

Lee, Y., Manegold, J. E., Kim, A. D., Pouget, C., Stachura, D. L., Clements, W. K. and Traver, D. (2014). FGF signalling specifies haematopoietic stem cells through its regulation of somitic Notch signalling. *Nat Commun* **5**, 5583.

Lenhart, K. F., Holtzman, N. G., Williams, J. R. and Burdine, R. D. (2013). Integration of nodal and BMP signals in the heart requires FoxH1 to create left-right differences in cell migration rates that direct cardiac asymmetry. *PLoS Genet* **9**, e1003109.

Long, S., Ahmad, N. and Rebagliati, M. (2003). The zebrafish nodal-related gene southpaw is required for visceral and diencephalic left-right asymmetry. *Development* **130**, 2303-2316.

Manner, J. (2004). On rotation, torsion, lateralization, and handedness of the embryonic heart loop: new insights from a simulation model for the heart loop of chick embryos. *Anat Rec A Discov Mol Cell Evol Biol* **278**, 481-492.

Marques, S. R., Lee, Y., Poss, K. D. and Yelon, D. (2008). Reiterative roles for FGF signaling in the establishment of size and proportion of the zebrafish heart. *Dev Biol* **321**, 397-406.

Massague, J. (2003). Integration of Smad and MAPK pathways: a link and a linker revisited. *Genes Dev* **17**, 2993-2997.

Mohammadi, M., McMahon, G., Sun, L., Tang, C., Hirth, P., Yeh, B. K., Hubbard, S. R. and Schlessinger, J. (1997). Structures of the tyrosine kinase domain of fibroblast growth factor receptor in complex with inhibitors. *Science* **276**, 955-960.

Nasevicius, A. and Ekker, S. C. (2000). Effective targeted gene 'knockdown' in zebrafish. *Nat Genet* **26**, 216-220.

Navarrete, I. A. and Levine, M. (2016). Nodal and FGF coordinate ascidian neural tube morphogenesis. *Development* **143**, 4665-4675.

634 **Nevis, K., Obregon, P., Walsh, C., Guner-Ataman, B., Burns, C. G. and Burns, C. E.** (2013). Tbx1
635 is required for second heart field proliferation in zebrafish. *Dev Dyn* **242**, 550-559.
636 **Nguyen, C. T., Lu, Q., Wang, Y. and Chen, J. N.** (2008). Zebrafish as a model for cardiovascular
637 development and disease. *Drug Discov Today Dis Models* **5**, 135-140.
638 **Noel, E. S., Verhoeven, M., Lagendijk, A. K., Tessadori, F., Smith, K., Choorapoikayil, S., den**
639 **Hertog, J. and Bakkers, J.** (2013). A Nodal-independent and tissue-intrinsic mechanism
640 controls heart-looping chirality. *Nat Commun* **4**, 2754.
641 **Patel, A. L., Yeung, E., McGuire, S. E., Wu, A. Y., Toettcher, J. E., Burdine, R. D. and Shvartsman,**
642 **S. Y.** (2019). Optimizing photoswitchable MEK. *Proc Natl Acad Sci U S A* **116**, 25756-25763.
643 **Pouget, C., Peterkin, T., Simoes, F. C., Lee, Y., Traver, D. and Patient, R.** (2014). FGF signalling
644 restricts haematopoietic stem cell specification via modulation of the BMP pathway. *Nat*
645 *Commun* **5**, 5588.
646 **Regan, J. C., Concha, M. L., Roussigne, M., Russell, C. and Wilson, S. W.** (2009). An Fgf8-
647 dependent bistable cell migratory event establishes CNS asymmetry. *Neuron* **61**, 27-34.
648 **Reifers, F., Bohli, H., Walsh, E. C., Crossley, P. H., Stainier, D. Y. and Brand, M.** (1998). Fgf8 is
649 mutated in zebrafish acerebellar (ace) mutants and is required for maintenance of midbrain-
650 hindbrain boundary development and somitogenesis. *Development* **125**, 2381-2395.
651 **Reifers, F., Walsh, E. C., Leger, S., Stainier, D. Y. and Brand, M.** (2000). Induction and differentiation
652 of the zebrafish heart requires fibroblast growth factor 8 (fgf8/acerebellar). *Development* **127**,
653 225-235.
654 **Reischauer, S., Arnaout, R., Ramadass, R. and Stainier, D. Y.** (2014). Actin binding GFP allows 4D
655 in vivo imaging of myofilament dynamics in the zebrafish heart and the identification of Erbb2
656 signaling as a remodeling factor of myofibril architecture. *Circ Res* **115**, 845-856.
657 **Riedl, J., Crevenna, A. H., Kessenbrock, K., Yu, J. H., Neukirchen, D., Bista, M., Bradke, F.,**
658 **Jenne, D., Holak, T. A., Werb, Z., et al.** (2008). Lifeact: a versatile marker to visualize F-actin.
659 *Nat Methods* **5**, 605-607.
660 **Rohr, S., Bit-Avragim, N. and Abdelilah-Seyfried, S.** (2006). Heart and soul/PRKCi and nagie
661 oko/Mpp5 regulate myocardial coherence and remodeling during cardiac morphogenesis.
662 *Development* **133**, 107-115.
663 **Rohr, S., Otten, C. and Abdelilah-Seyfried, S.** (2008). Asymmetric involution of the myocardial field
664 drives heart tube formation in zebrafish. *Circ Res* **102**, e12-19.
665 **Roussigne, M., Wei, L., Tsingos, E., Kuchling, F., Alkobtawi, M., Tsalavouta, M., Wittbrodt, J.,**
666 **Carl, M., Blader, P. and Wilson, S. W.** (2018). Left/right asymmetric collective migration of
667 parapineal cells is mediated by focal FGF signaling activity in leading cells. *Proc Natl Acad Sci*
668 *U S A* **115**, E9812-E9821.
669 **Schaks, M., Giannone, G. and Rottner, K.** (2019). Actin dynamics in cell migration. *Essays in*
670 *Biochemistry* **63**, 483-495.
671 **Schier, A. F.** (2009). Nodal morphogens. *Cold Spring Harb Perspect Biol* **1**, a003459.
672 **Shu, X., Cheng, K., Patel, N., Chen, F., Joseph, E., Tsai, H. J. and Chen, J. N.** (2003). Na,K-ATPase
673 is essential for embryonic heart development in the zebrafish. *Development* **130**, 6165-6173.
674 **Smith, K. A., Chocron, S., von der Hardt, S., de Pater, E., Soufan, A., Bussmann, J., Schulte-**
675 **Merker, S., Hammerschmidt, M. and Bakkers, J.** (2008). Rotation and asymmetric
676 development of the zebrafish heart requires directed migration of cardiac progenitor cells. *Dev*
677 *Cell* **14**, 287-297.
678 **Smith, K. A. and Uribe, V.** (2021). Getting to the Heart of Left-Right Asymmetry: Contributions from
679 the Zebrafish Model. *J Cardiovasc Dev Dis* **8**.
680 **Stainier, D. Y. R., Raz, E., Lawson, N. D., Ekker, S. C., Burdine, R. D., Eisen, J. S., Ingham, P. W.,**
681 **Schulte-Merker, S., Yelon, D., Weinstein, B. M., et al.** (2017). Guidelines for morpholino use
682 in zebrafish. *PLoS Genet* **13**, e1007000.
683 **Thisse, B. and Thisse, C.** (2014). In situ hybridization on whole-mount zebrafish embryos and young
684 larvae. *Methods Mol Biol* **1211**, 53-67.
685 **Trinh, L. A. and Stainier, D. Y.** (2004). Fibronectin regulates epithelial organization during myocardial
686 migration in zebrafish. *Dev Cell* **6**, 371-382.

687 **Tsao, C. W., Aday, A. W., Almarzooq, Z. I., Alonso, A., Beaton, A. Z., Bittencourt, M. S., Boehme,**
688 **A. K., Buxton, A. E., Carson, A. P., Commodore-Mensah, Y., et al.** (2022). Heart Disease
689 and Stroke Statistics-2022 Update: A Report From the American Heart Association. *Circulation*
690 **145**, e153-e639.
691 **Veerkamp, J., Rudolph, F., Cseresnyes, Z., Priller, F., Otten, C., Renz, M., Schaefer, L. and**
692 **Abdelilah-Seyfried, S.** (2013). Unilateral dampening of Bmp activity by nodal generates cardiac
693 left-right asymmetry. *Dev Cell* **24**, 660-667.
694 **Vemaraju, S., Kantarci, H., Padanad, M. S. and Riley, B. B.** (2012). A spatial and temporal gradient
695 of Fgf differentially regulates distinct stages of neural development in the zebrafish inner ear.
696 *PLoS Genet* **8**, e1003068.
697 **Witzel, H. R., Cheedipudi, S., Gao, R., Stainier, D. Y. and Dobreva, G. D.** (2017). Isl2b regulates
698 anterior second heart field development in zebrafish. *Sci Rep* **7**, 41043.
699 **Woo, S., Housley, M. P., Weiner, O. D. and Stainier, D. Y.** (2012). Nodal signaling regulates
700 endodermal cell motility and actin dynamics via Rac1 and Prex1. *J Cell Biol* **198**, 941-952.
701 **Yelon, D., Horne, S. A. and Stainier, D. Y.** (1999). Restricted expression of cardiac myosin genes
702 reveals regulated aspects of heart tube assembly in zebrafish. *Dev Biol* **214**, 23-37.
703 **Zhou, Y., Cashman, T. J., Nevis, K. R., Obregon, P., Carney, S. A., Liu, Y., Gu, A., Mosimann, C.,**
704 **Sondalle, S., Peterson, R. E., et al.** (2011). Latent TGF-beta binding protein 3 identifies a
705 second heart field in zebrafish. *Nature* **474**, 645-648.

706

707 **<u>Figure legends</u>**

708 **Figure 1. FGF signaling is active in the developing heart and necessary for proper heart**
709 **development.** (**A**) RNA *in situ* hybridization (ISH) by hybridization chain reaction (HCR) for *fgf8*
710 (magenta) and *myl7* (green) in the cardiac cone of a 20 hours post fertilization (hpf) wild-type (WT)
711 embryo. Scale = 25 µm. (**B**) Representative images of 5 days post fertilization (dpf) WT embryos or
712 embryos treated with FGF inhibitor SU5402 from 24-30 hpf (ventricle in magenta, atrium in cyan).
713 SU5402-treated embryos display aberrant cardiac looping, blood pooling at the sinus venosus, and
714 pericardial edema (lateral view) as well as the atrium failing to migrate behind the ventricle (ventral
715 view). (**C**) ISH for Nodal target gene *lefty2* in the cardiac cone of 20 hpf embryos shows correct left-
716 sided *lefty2* and incorrect right, bilateral, and absent *lefty2* expression. (**D**) Quantification of *lefty2*
717 expression sidedness. n is WT = 74, *ntl*$^{-/-}$ = 50, *spaw*$^{-/-}$ = 36, SU5402 = 41, *dn-fgfr1* = 20, *ntl*$^{-/-}$ + SU5402
718 = 177, *spaw*$^{-/-}$ + SU5402 = 63. Statistical significance was determined by Chi-square analysis. (**A, C**)
719 Images are dorsal views, with anterior to the top and left to the reader's left. ns = not significant, *** =
720 p<0.0001.

721

722 **Figure 2. FGF signaling is necessary for proper CPC migration but not cardiac laterality during**
723 **jogging.** (**A**) Schematization depicting the 18.5-24 hpf SU5402 treatment window during the "Cone
724 Formation and Jogging phase". (**B**) RNA ISH for *myl7* at 26.5 hpf visualizing correct left-sided
725 positioning and incorrect midline and right-sided positioning of the heart tube. (**C**) Quantification of
726 cardiac laterality phenotypes. n is WT = 534, *ntl*$^{-/-}$ = 113, *spaw*$^{-/-}$ = 138, SU5402 = 112, *dn-fgfr1* = 75, *ntl*$^{-}$
727 $^{/-}$ + SU5402 = 12, *spaw*$^{-/-}$ + SU5402 = 30, *spaw*$^{-/-}$ + MEK = 14; Chi-square analysis. (**D**) RNA ISH for
728 *myl7* at 24 hpf displaying the stages from cone through extending to correctly jogged heart tubes we

729 see in our treated embryos. (**E**) Quantification of cardiac migration phenotypes. Number of embryos (n)
730 is WT = 686, *ntl*$^{-/-}$ = 152, *spaw*$^{-/-}$ = 171, SU5402 = 531, *dn-fgfr1* = 225, *ntl*$^{-/-}$ + SU5402 = 117, *spaw*$^{-/-}$ +
731 SU5402 = 146, *spaw*$^{-/-}$ + MEK = 35; Chi-square analysis. (**F**) Quantification of heart tube length at 26.5
732 hpf. n is WT = 84, *spaw*$^{-/-}$ = 62, SU5402 = 80, *spaw*$^{-/-}$ + SU5402 = 9. Statistical significance determined
733 by Student's t-test. (**B, D**) Images are dorsal views, with anterior to the top and left to the reader's left.
734 ns = not significant, * = p<0.05, ** = p<.001, *** = p<0.0001.
735
736 **Figure 3. FGF signaling promotes CPC migration while Nodal promotes CPC migration and**
737 **laterality during jogging.** (**A**) Schematization of imaging strategy for time-lapse imaging of the cardiac
738 cone throughout jogging, with outer atrial cells in light green and inner ventricular cells in dark green.
739 Left-sided (blue) and right-sided (orange) cells that underwent tracking for analysis are shown. (**B**)
740 Representative time-lapse images depicting cardiac progenitor cell (CPC) migration from the formation
741 of the cardiac cone through the next 3 hours of development. WT and *ntl*$^{-/-}$ embryos typically complete
742 jogging and tube formation in this timeframe. Arrows indicate heart tube direction. Scale = 50 μm. (**C**)
743 Trajectories of left-sided (blue) and right-sided (orange) CPCs during 3 hours of jogging. Scale = 50
744 μm. (**D**) Rose plots demonstrating the angle of displacement of each tracked left-sided (blue) and right-
745 sided (orange) CPC after 3 hours of jogging. (**E**) Average velocity of left-sided and right-sided CPCs
746 during 3 hours of jogging; Student's t-test. (**C-E**) n = 3 embryos (5 left-sided and 5 right-sided cells
747 tracked per embryo) per condition. (**B-C**) Images are dorsal views, with anterior to the top and left to the
748 reader's left. ns = not significant, * = p<.05, *** = p<0.0001.
749
750 **Figure 4. F-actin dynamics are asymmetric and Nodal-dependent in CPCs during jogging.** (**A**)
751 *Tg(myl7:Lifeact-EGFP)* embryo at 24 hpf demonstrating the fluorescence of the CPCs composing the
752 heart tube. (**B**) F-actin protrusions (pink asterisks) in a singular CPC of a mosaic *Tg(myl7:Lifeact-*
753 *EGFP)* embryo at 21 hpf. (**C**) F-actin protrusive activity in left (blue box) compared to right (orange box)
754 CPCs in the cardiac cone of a *Tg(myl7:Lifeact-EGFP)* embryo over the course of jogging from 19-23
755 hpf. (**D**) Cardiac cones of *Tg(myl7:Lifeact-EGFP)* WT, *ntl* morphant, *spaw* morphant, and SB505124-
756 treated embryos, with left-sided (blue oval) and right-sided (orange oval) atrial CPCs marked. (**E**)
757 Fluorescence intensity ratio between left-sided and right-sided CPCs. n is WT = 4, *ntl* MO = 4, *spaw*
758 MO = 7, SB-505124 = 5; Student's t-test. (**F**) Cardiac cones of *Tg(myl7:GFP-UtrCH)* WT and SU5402-
759 treated embryos. (**G**) Quantification of mean fluorescence intensity. (**A-D, F**) Images are dorsal views,
760 with anterior to the top and left to the reader's left. ns = not significant, * = p<0.05.
761
762 **Figure 5. FGF signaling is necessary for SHF addition and proper cardiac looping.** (**A**)
763 Schematization depicting the SU5402 treatment windows during the "Elongation phase" from 24-30 hpf,
764 the "Bending phase" from 30-36 hpf, and the "Continuous treatment" window from 24-48 hpf. (**B**)

765 Representative images of WT, SU5402-treated, *spaw*$^{-/-}$*, and ltbp3* morphant *Tg(myl7:EGFP)* embryo
766 hearts at 48 hpf, depicting how the looping angle is measured (pink lines; AP = anterior/poster axis line
767 and AVC = line through the AVC). (**C**) Quantification of looping laterality phenotypes. n is WT = 70,
768 SU5402 elongation phase = 40, SU5402 bending phase = 50, *spaw*$^{-/-}$ = 53, *spaw*$^{-/-}$ + SU5402
769 elongation phase = 22; Chi-square analysis. (**D**) Quantification of looping angle . n is WT = 38, SU5402
770 elongation phase = 39, SU5402 bending phase = 50, *spaw*$^{-/-}$ = 53, *spaw*$^{-/-}$ + SU5402 elongation phase
771 = 22, *ltbp3* MO = 50; Student's t-test. (**E**) Quantification of heart tube length in WT and SU5402-treated
772 *Tg(nkx2.5:ZsYellow)* embryo heart tubes at 26.5 or 28 hpf. n is WT 26.5 hpf = 24, SU5402 26.5 hpf = 7,
773 WT 28 hpf = 13, SU5402 28 hpf = 19; Student's t-test. (**B**) Images are ventral views, with anterior to the
774 top and left to the reader's right. ns = not significant, * = $p<0.05$, *** = $p<0.0001$.
775
776 **Figure 6. Model of the synergistic and distinct roles of Nodal and FGF signaling in asymmetric**
777 **cardiac morphogenesis.**
778 In the cardiac cone, Nodal and FGF signaling impinges on the actin cytoskeleton to promote CPC
779 migration during jogging. Nodal promotes a left-lateralized migration to generate cardiac asymmetry,
780 while FGF promotes a permissive migration in all CPCs. Next, in the heart tube, both Nodal and FGF
781 signals promote proper cardiac looping. Nodal promotes looping laterality to correctly position the
782 chambers, while FGF induces the SHF which, in turn, is likely necessary for robust looping. The looped
783 heart then matures to form a two-chambered heart by 48 hpf.

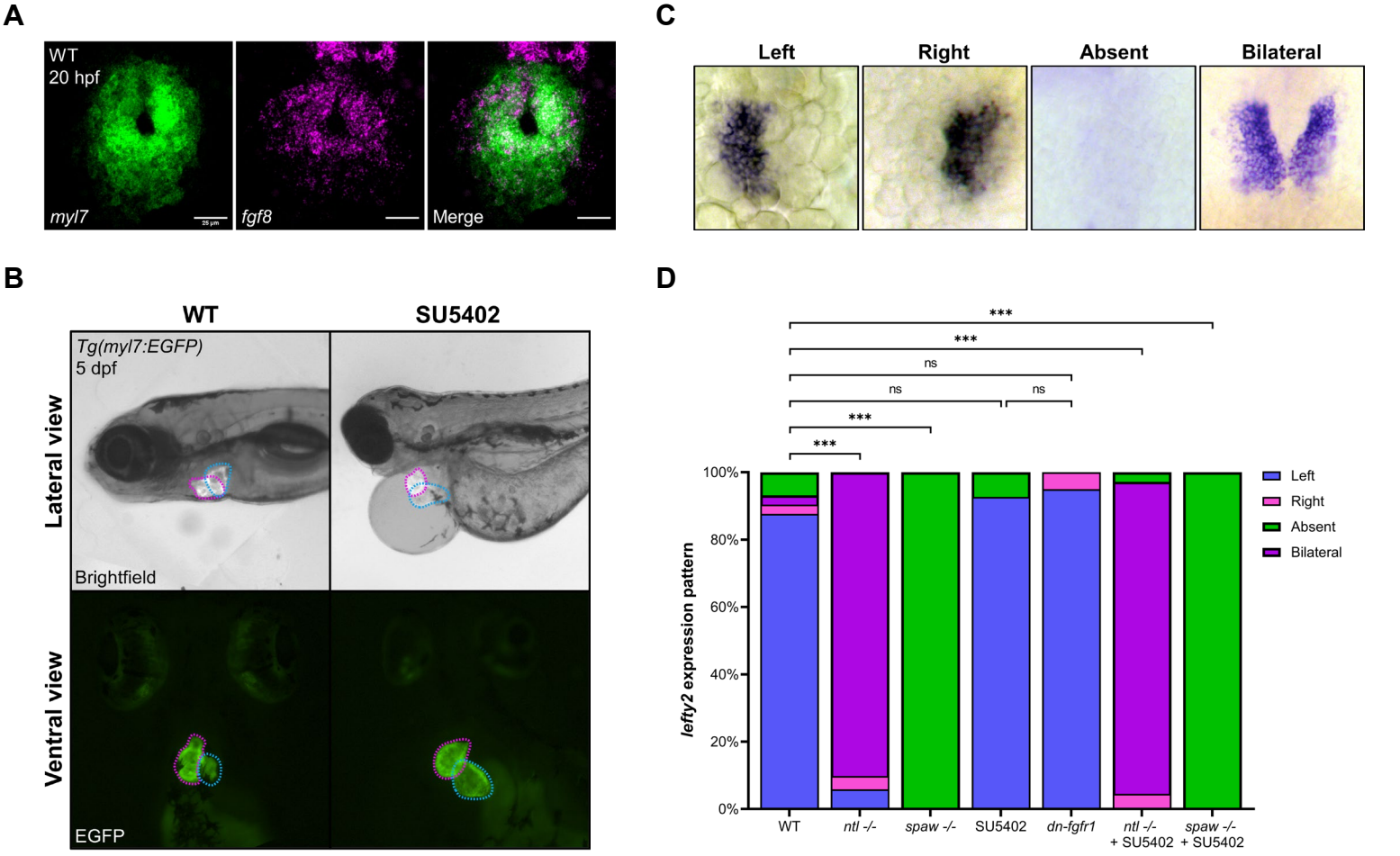
A
WT
20 hpf
myl7
fgf8
Merge
C
Left
Right
Absent
Bilateral
B
WT
SU5402
Tg(myl7:EGFP)
5 dpf
Lateral view
Brightfield
Ventral view
EGFP
D
***
***
ns
ns
ns
***
***
100%
80%
60%
40%
20%
0%
lefty2 expression pattern
Left
Right
Absent
Bilateral
WT
ntl -/-
spaw -/-
SU5402
dn-fgfr1
ntl -/- + SU5402
spaw -/- + SU5402

Figure 1.

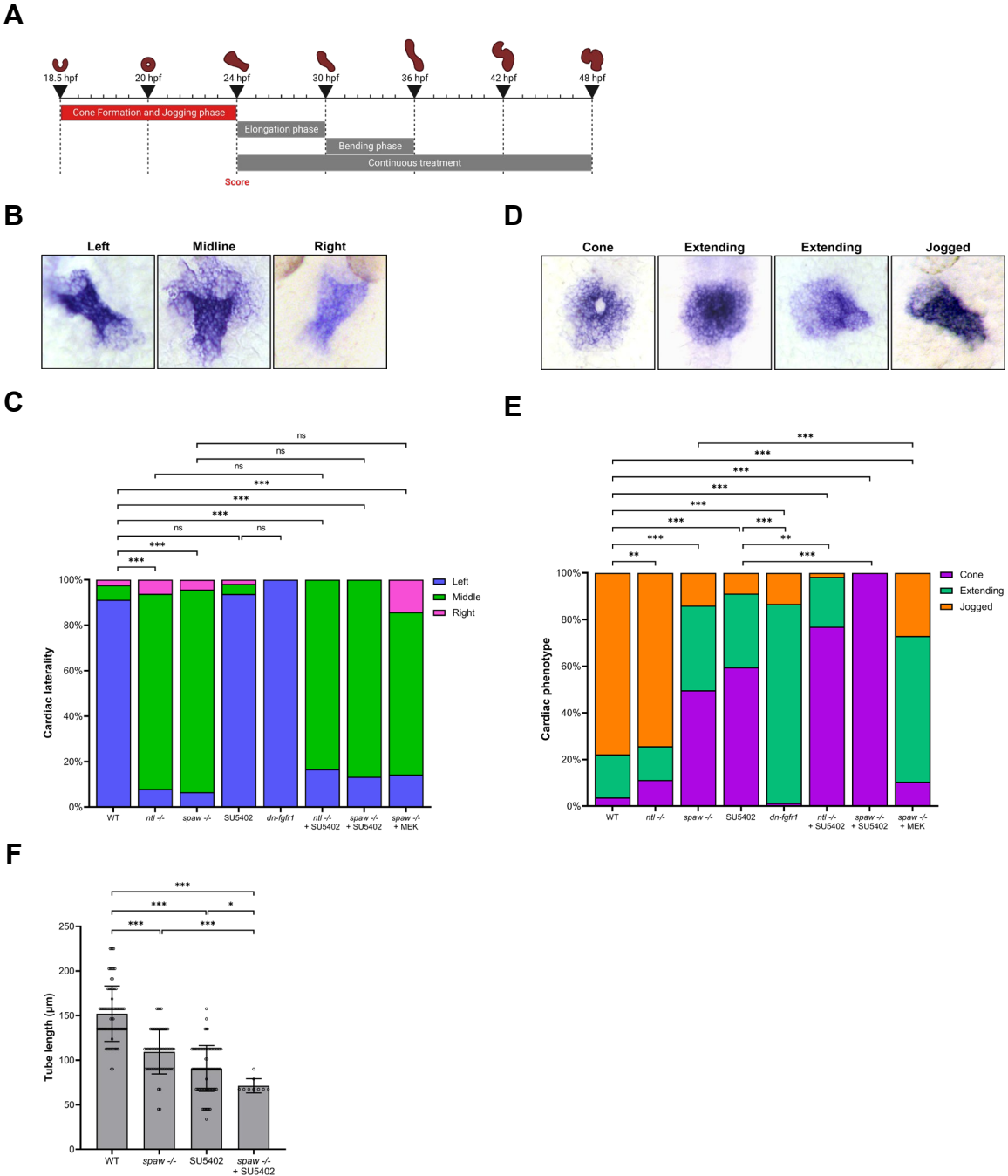
A
18.5 hpf
20 hpf
24 hpf
30 hpf
36 hpf
42 hpf
48 hpf
Cone Formation and Jogging phase
Elongation phase
Bending phase
Continuous treatment
Score
B
Left
Midline
Right
D
Cone
Extending
Extending
Jogged
C
Cardiac laterality
100%
80%
60%
40%
20%
0%
Left
Middle
Right
WT
ntl -/-
spaw -/-
SU5402
dn-fgfr1
ntl -/- + SU5402
spaw -/- + SU5402
spaw -/- + MEK
E
Cardiac phenotype
Cone
Extending
Jogged
F
Tube length (µm)
250
200
150
100
50
0
WT
spaw -/-
SU5402
spaw -/- + SU5402

Figure 2.

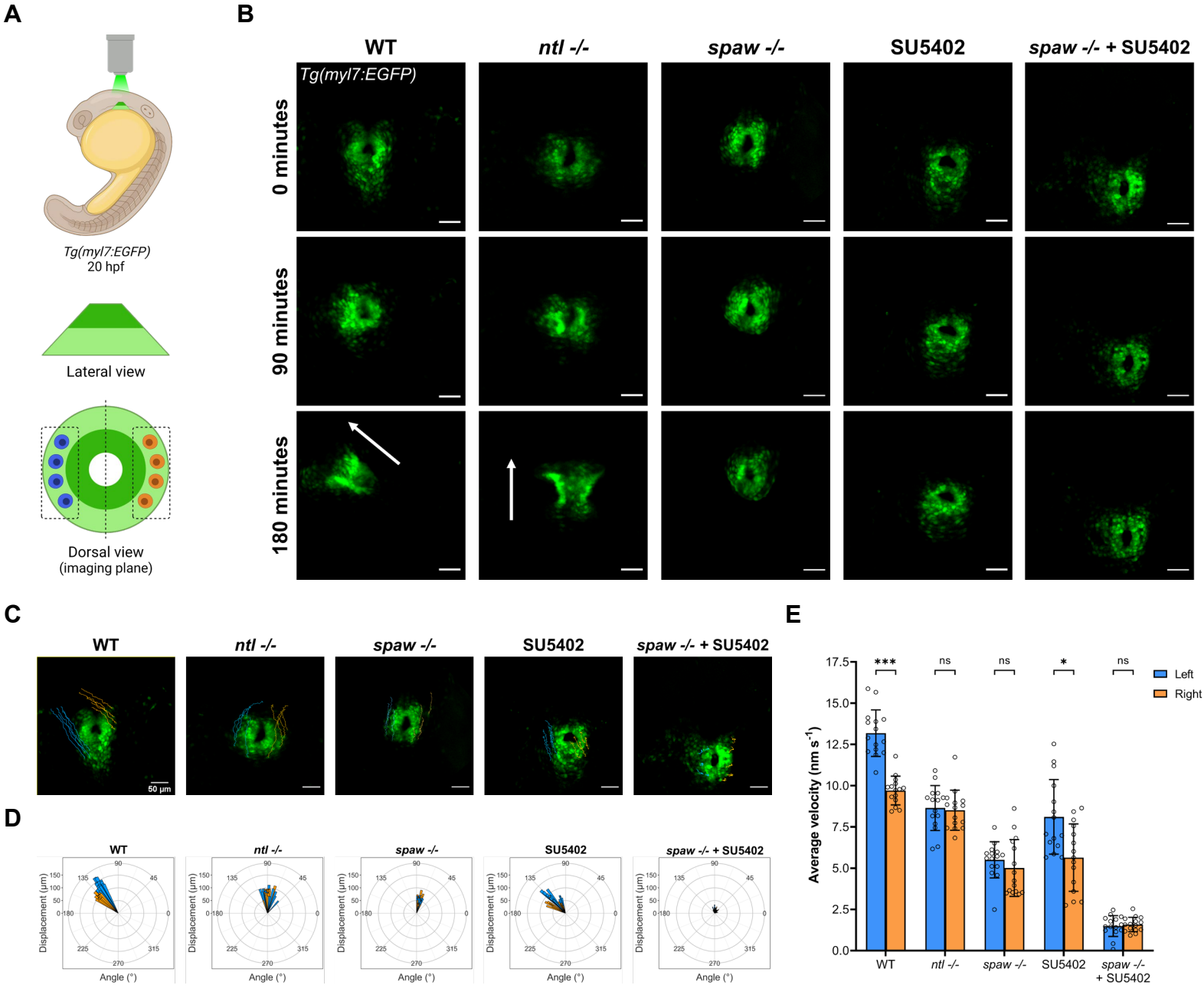
A
Tg(myl7:EGFP)
20 hpf
Lateral view
Dorsal view
(imaging plane)
B
WT
ntl -/-
spaw -/-
SU5402
spaw -/- + SU5402
Tg(myl7:EGFP)
0 minutes
90 minutes
180 minutes
C
WT
ntl -/-
spaw -/-
SU5402
spaw -/- + SU5402
50 µm
D
WT
ntl -/-
spaw -/-
SU5402
spaw -/- + SU5402
Displacement (µm)
Angle (°)
E
Average velocity (nm s-1)
Left
Right
***
ns
ns
*
ns
WT
ntl -/-
spaw -/-
SU5402
spaw -/- + SU5402

Figure 3.

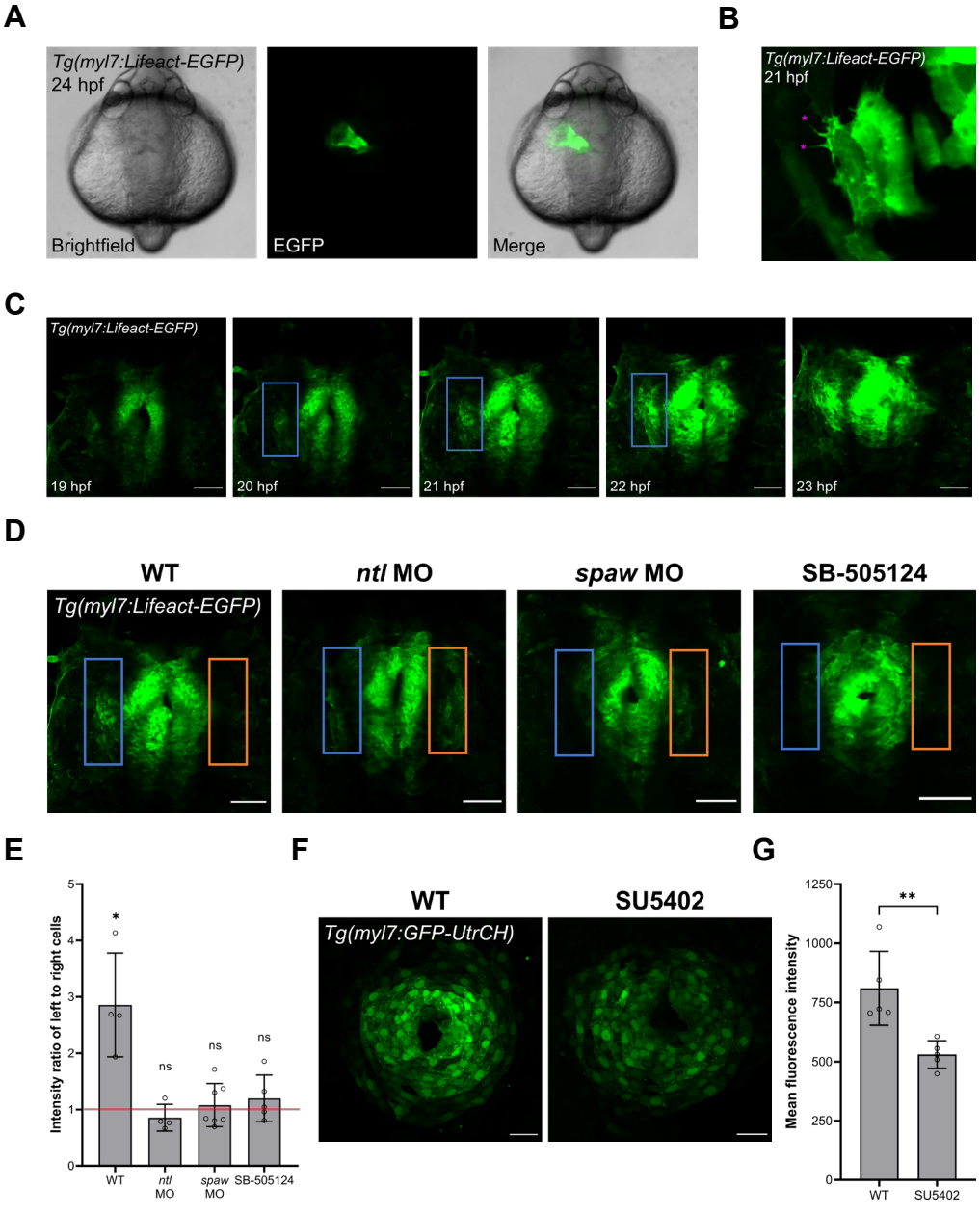
A
Tg(myl7:Lifeact-EGFP)
24 hpf
Brightfield
EGFP
Merge
B
Tg(myl7:Lifeact-EGFP)
21 hpf
C
Tg(myl7:Lifeact-EGFP)
19 hpf
20 hpf
21 hpf
22 hpf
23 hpf
D
WT
ntl MO
spaw MO
SB-505124
Tg(myl7:Lifeact-EGFP)
E
Intensity ratio of left to right cells
WT
ntl MO
spaw MO
SB-505124
ns
*
F
WT
SU5402
Tg(myl7:GFP-UtrCH)
G
Mean fluorescence intensity
WT
SU5402
**

Figure 4.

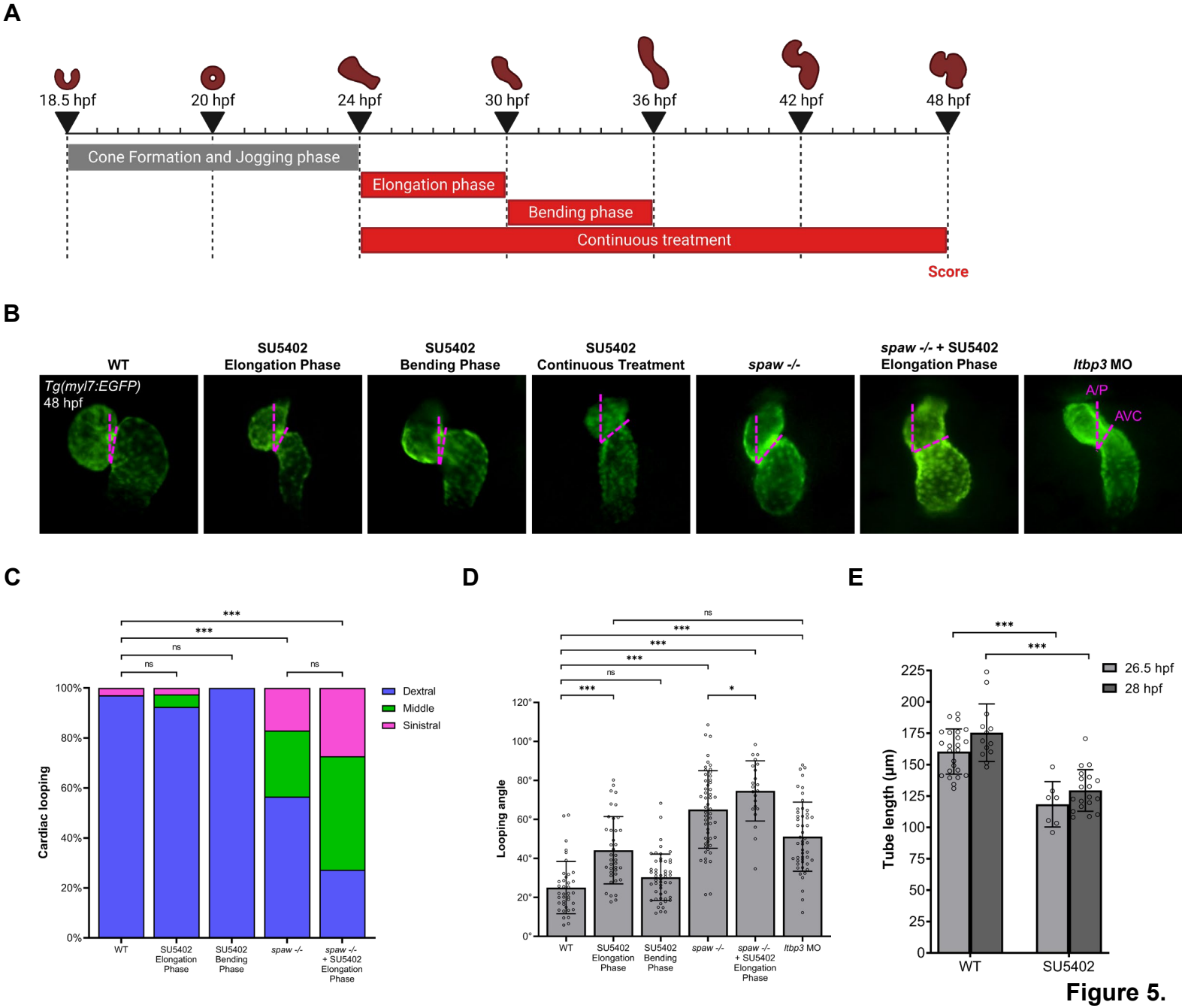
A
18.5 hpf
20 hpf
24 hpf
30 hpf
36 hpf
42 hpf
48 hpf
Cone Formation and Jogging phase
Elongation phase
Bending phase
Continuous treatment
Score
B
WT
SU5402 Elongation Phase
SU5402 Bending Phase
SU5402 Continuous Treatment
spaw -/-
spaw -/- + SU5402 Elongation Phase
ltbp3 MO
Tg(myl7:EGFP)
48 hpf
A/P
AVC
C
Cardiac looping
100%
80%
60%
40%
20%
0%
Dextral
Middle
Sinistral
WT
SU5402 Elongation Phase
SU5402 Bending Phase
spaw -/-
spaw -/- + SU5402 Elongation Phase
***
ns
D
Looping angle
120°
100°
80°
60°
40°
20°
0°
*
E
Tube length (µm)
225
200
175
150
125
100
75
50
25
0
26.5 hpf
28 hpf
WT
SU5402

Figure 5.

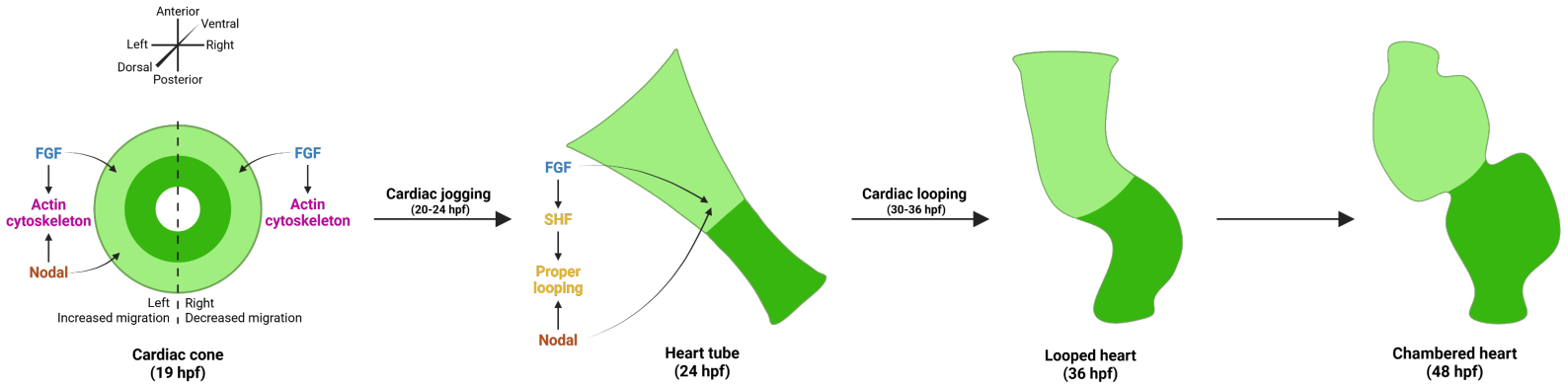
Anterior
Ventral
Left
Right
Dorsal
Posterior
FGF
Actin cytoskeleton
Nodal
FGF
Actin cytoskeleton
Left
Right
Increased migration
Decreased migration
Cardiac cone
(19 hpf)
Cardiac jogging
(20-24 hpf)
FGF
SHF
Proper looping
Nodal
Heart tube
(24 hpf)
Cardiac looping
(30-36 hpf)
Looped heart
(36 hpf)
Chambered heart
(48 hpf)

Figure 6.